FARADAY

Preparation and crystallinity of a large unsubstituted crown ether, cyclic heptacosa(oxyethylene) (*cyclo*-E_{27}, 81-crown-27), studied by Raman spectroscopy, X-ray scattering and differential scanning calorimetry

Zhuo Yang,[a] Ga-Er Yu,[a] Jennifer Cooke,[b] Ziad Ali-Adib,[a] Kyriakos Viras,[a]† Hiroatsu Matsuura,[a]‡ Anthony J Ryan[b,c] and Colin Booth[a]

[a] *Manchester Polymer Centre, Department of Chemistry, University of Manchester, Manchester, UK M13 9PL*

[b] *Manchester Materials Science Centre, UMIST, Grosvenor Street, Manchester, UK M1 7HS*

[c] *CCLRC, Daresbury Laboratory, Warrington, UK WA4 4AD*

Cyclic heptacosa(oxyethylene) (*cyclo*-E_{27}, 81-crown-27) was prepared from linear α-hydro, ω-hydroxy-heptacosa(oxyethylene) by reaction with tosyl chloride under alkaline conditions, purified by preparative-scale gel permeation chromatography, and studied by laser-Raman spectroscopy, wide-angle and small-angle X-ray scattering, and differential scanning calorimetry. Comparison was made with the properties of linear oligo(oxyethylene) dimethyl ethers (including $C_1E_{27}C_1$). The sub-cell of the crystalline cyclic oligomer was the same as that of its linear counterparts, *i.e.* the same as that of high-molar-mass poly(oxyethylene). However, the cyclic oligomer crystallised as a twice-folded ring, as confirmed by its long spacing and the frequency of its single-node longitudinal acoustic mode (LAM-1). Enthalpies of fusion and melting temperatures were analysed to provide estimates of the enthalpy and entropy of formation of a fold in an oligo(oxyethylene) layer crystal.

1. Introduction

Many linear and cyclic oligomers have been prepared, as summarised in the extensive tables in the Polymer Handbook.[1] Here we use the term oligomer in the same sense as Rothe and Rothe[1] to mean a uniform sample with all molecules the same length. Nevertheless there are few reports of comparative studies of the crystallinity of cyclic and linear oligomers of similar chain length: examples are studies by Wegner and coworkers[2–4] of large linear and cyclic alkanes, and by Höcker and coworkers[5] of large linear and cyclic oligourethanes. There has been recent interest[6–8] in the preparation of large unsubstituted cyclic oligo(oxyethylene)s, *i.e.* large crown ethers but so far as we are aware this detailed report of the purification and crystallinity of a large crown ether (*cyclo*-E_{27}, 81-crown-27) is the first of its kind. Here and elsewhere E denotes an oxyethylene unit (OCH_2CH_2).

Lengthy uniform dihydroxy-ended oligo(oxyethylene)s with chain lengths up to E_{60} have been prepared[9–14] and studied with respect to crystallinity by a number of techniques, including differential scanning calorimetry (DSC), wide- and small-angle X-ray scattering (WAXS and SAXS), and high- and low-frequency Raman spectroscopy.[15–19] Chain folding on crystallisation at or about room temperature was identified[20] in oligo(oxyethylene) dialkyl ethers of chain length approximately 170 chain atoms, *i.e.* much the same chain length as found for the lengthy *n*-alkanes under similar conditions.[2,21] Our present interest in large cyclic oligo(oxyethylene)s can be judged against this background, since rings above a certain size must crystallise with parallel stems connected by folds.

Comparative studies of the crystallinity of non-uniform cyclic and linear poly(oxyethylene)s have been reported recently.[22–24] These cyclic polymers were prepared from polyethylene glycols by reaction at extreme dilution under alkaline conditions, with either dichloromethane or tosyl chloride,[24–26] ring closure being effected by formation of either an acetal or an ether link:

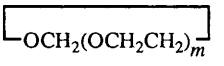

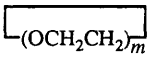

The cyclic polymers studied[22–24] had number-average molar masses (M_n) in the range 1000–3000 g mol^{-1} (*i.e* number-average $m \approx 23$–68) and narrow molar mass distributions ($M_w/M_n < 1.1$). It was confirmed by WAXS and high-frequency Raman spectroscopy that they crystallised in the usual way,[27] *i.e.* as alternate right- and left-handed helices forming a monoclinic sub-cell, and by SAXS and low-frequency Raman spectroscopy that they adopted the expected twice-folded conformation, as indicated below

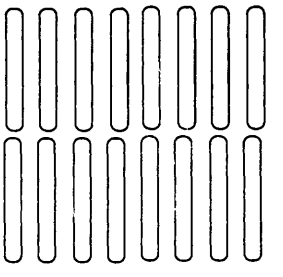

Since the use of non-uniform chains necessarily introduces uncertainty into the interpretation of the experimental results, particularly through the possibility of fractionation during crystallisation, it was decided to carry out similar studies with uniform samples of linear and cyclic oligo(oxyethylene). The work reported below forms a part of that scheme. Since the aim was to compare linear and cyclic oligo(oxyethylene)s, the method used was to prepare linear hydroxy-ended

† Visiting fellow. Permanent address: National and Kapodistrian University of Athens, Department of Chemistry, Physical Chemistry, Laboratory, Panepistimiopolis, 157 71 Athens, Greece

‡ Visiting fellow. Permanent address: Department of Chemistry, Faculty of Science, Hiroshima University, Kagamiyama, Higashi-Hiroshima 739, Japan.

oligo(oxyethylene) with 27 oxyethylene units, samples of which were either cyclised by ether closure or methylated. The following notation is used for the three compounds:

E_{27}	linear chain, dihydroxy ended
$C_1E_{27}C_1$	linear chain, dimethyl ether
cyclo-E_{27}	cyclic ether (81-crown-27).

Other oligomers obtained during the work as precursors or by-products are denoted in a similar way.

2. Preparation of linear and cyclic oligomers

The syntheses started from triethylene glycol [α-hydro, ω-hydroxytri(oxyethylene)] and proceeded *via* a chain extension reaction (much as described by Bömer *et al.*[9]) first to the nonamer (E_9) and then (in a second extension) to the heptacosamer (E_{27}). The general method of chain extension was reaction of *p*-tolylsulfonyl chloride (tosyl chloride) with the glycol to form the ditosylate, and subsequent reaction with the monopotassium salt of the same glycol to obtain a product of three times the original chain length. A number of methods have been proposed for efficient tosylation of a glycol. Previously we carried out the esterification reaction either in dry pyridine[10–12] or in dichloromethane plus triethylamine,[28] the latter method being a modification of that of De Vos and Goethals.[29] Yields were generally satisfactory: *e.g.* 88%.[28] In the present work the method advocated by Ouchi *et al.*[30] was used.

2.1 Analytical gel permeation chromatography

GPC was used extensively to monitor the preparation and purification of the samples and to confirm the purity of the samples actually studied by DSC, WAXS/SAXS and Raman spectroscopy. The eluent was tetrahydrofuran at 25 °C at a flow rate of 1 cm^3 min^{-1}. Detection was by differential refractometry. Samples (concentration 1–2 g dm^{-3}) were injected *via* a 100 mm^3 loop. System A, which had one 60 cm PL-gel column of nominal porosity 50 Å, was used to monitor the preparation of oligomer E_{27}. System B, which had three 30 cm columns packed with Styragel (HR1, HR2, HR3) and so improved resolution in the higher size range, was used to check the cyclic and linear samples as they were finally purified. Both systems were calibrated using the linear and cyclic oligo(oxyethylene)s prepared the present work. A sample of *cyclo*-E_{10} prepared in Prof. Gibson's laboratory was also included. The calibrations was also checked against those obtained for the same systems using linear and cyclic poly(oxyethylene)s with narrow chain length distributions and number-average molar masses 1000 to 3000 g mol^{-1}, as described previously.[24] Calibration curves obtained for GPC System B are shown in Fig. 1. The difference in elution volume between linear and cyclic samples of the same chain length is much as expected.[24,31]

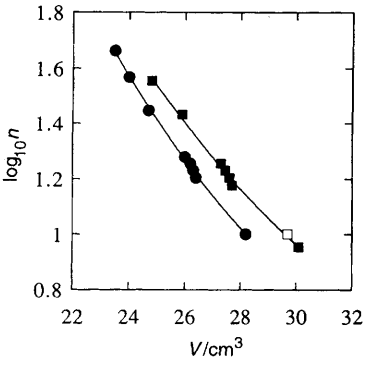

Fig. 1 Calibration curves for GPC System B. Logarithm of chain length in E units, *i.e.* *n* for (●) cyclic oligomers and $n + 1$ for (■) linear oligomers, *vs.* elution volume (*V*). (□) Denotes a sample of *cyclo*-E_{10} prepared in Prof. Gibson's laboratory.

2.2 Materials

Triethylene glycol (Fluka, 99%) was dried over anhydrous $MgSO_4$ for several days before collecting a fraction distilled at reduced pressure (b.p. 94–100 °C at 0.1 mm Hg). When needed, tetrahydrofuran (BDH, THF) was dried over CaH_2 (reflux) and then distilled onto type 4A molecular sieves for storage. Other reagents and solvents were used as received. The KOH contained 15 mass% water.

2.2 α-Hydro, ω-hydroxynona(oxyethylene) (E_9)

Sodium hydroxide (40.0 g, 1.0 mol) was dissolved in water (200 cm^3) and a solution of triethylene glycol (52.6 g, 0.35 mol) in tetrahydrofuran (THF, 150 cm^3) was added. This mixture was cooled to 0 °C and a solution of tosyl chloride (133.5 g, 0.70 mol) was added with stirring over a period of 2 h. After stirring for an additional 2 h at 0 °C, the mixture was poured into ice–water (2 dm^3). The resulting precipitate was removed by filtration, and the filtrate washed with water (2 × 500 cm^3) and finally dried under vacuum (20 °C, 0.01 mm Hg, 16 h). Recrystallisation from methanol was used to ensure high purity. The yield was 80%, the m.p. was 81.0–81.5 °C. The absence of absorption at 3600–3200 cm^{-1} in the infrared spectrum of the product indicated complete conversion to product, and bands at 1175 and 1190 cm^{-1} were consistent with formation of the ditosylate. The ^1H NMR spectrum (200 MHz, $CDCl_3$) showed the expected resonances and integrals.

A mixture of triethylene glycol (210 g, 1.4 mol) and KOH (85%, 31.7 g, 0.48 mol) was stirred and heated under vacuum (50 °C, 0.1 mm Hg, 5 h) to remove water and to form (mainly) the monopotassium salt as a viscous yellow liquid. A solution of triethylene glycol ditosylate (110.1 g, 0.24 mol) in dry THF (800 cm^3) was added, and the resulting solution was stirred in the dark at room temperature for 10 days. The white precipitate of potassium tosylate was removed by filtration, and the solvent by rotary evaporation. Distilled water (300 cm^3) was added to the residue and the cloudy mixture was gently refluxed (3 h) before removing additional potassium tosylate by filtration. The resulting clear solution was brought to pH = 6 (HCl) and extracted with dichloromethane (12 × 200 cm^3). Evaporation of the solvent yielded a yellow oil, shown by analytical GPC to contain a mixture of oligomeric glycols, principally E_9 (*ca.* 50 mass%) and unreacted starting material (E_3) plus smaller quantities of E_6 and E_{12}. GPC results typical of those obtained in the present work have been published previously.[10,11] The required oligomer E_9 was isolated from the crude product by short-path fractional distillation of batches of 30–40 g, as described previously.[10] Typically the final yield of pure E_9 was 20 mass%.

2.3 α-Hydro, ω-hydroxyheptacosa(oxyethylene) (E_{27})

The preparation of heptacosaethylene glycol (E_{27}) from E_9 was parallel to that described above up to the separation stage. The GPC curve of the crude product (see Fig. 2) indicated a conversion of E_9 to E_{27} of approximately 50% based on peak area. The principal oligomeric impurities in the crude product were E_{18}, E_{36} and E_{45}, as indicated in Fig. 2. Because of the low volatility of these oligomers, separation was carried out by preparative GPC using the system described previously,[11,12] *i.e.* one based on two columns, each 80 cm long and 2.5 cm i.d., packed with Sephadex LH-20 gel. Separation into four fractions gave samples which were judged pure enough to be used in the preparation of the cyclic oligomer and the dimethyl ether. As described below, the small fractions of higher oligomers were not resolved by GPC System A, but were resolved by System B and were removed

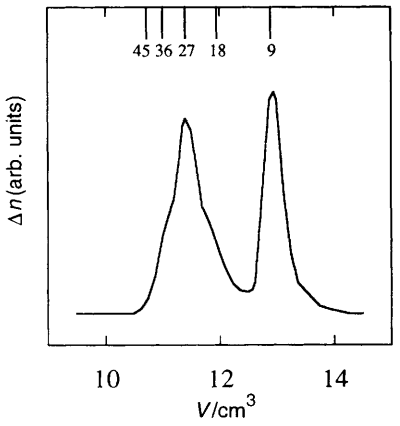

Fig. 2 GPC curve obtained using System A of the crude product from the preparation of linear oligomer E_{27}. The elution volumes of the main constituents (E_{27} and starting material E_9) are marked, together with the elution volumes of oligomeric impurities.

by preparative GPC at a later stage. About half of the E_{27} was lost in the purification, and a second preparation was carried out under identical conditions in order to obtain sufficient material for subsequent work.

2.4 *Cyclo*-heptacosa(oxyethylene) (*cyclo*-E_{27})

E_{27} (0.50 g) and an approximately equimolar amount of tosyl chloride was dissolved in THF (50 cm^3) and slowly added (over 48 h by syringe pump) to a dispersion of powdered KOH (2.5 g) in a mixture of THF and heptane (75/25 vol.%). The purpose of the poor solvent (heptane) was to optimise ring closure by reducing the average end-to-end distance of the oligomer coil. After stirring for a further 24 h in order to ensure essentially complete reaction of all end groups, the mixture was filtered and the solvent evaporated from the solution (initially by rotary evaporation, finally under vacuum, 10^{-4} mm Hg) to obtain a crude sample of *cyclo*-E_{27}, *i.e.* a mixture of the required product with cyclic and chain-extended linear oligomers.

Preparative GPC was used to obtain a first fraction denoted *cyclo*-E_{27}-1. GPC analysis (system B) of this sample revealed the presence of a higher oligomer with elution volume consistent with *cyclo*-E_{36}: see curve (*a*) in Fig. 3.

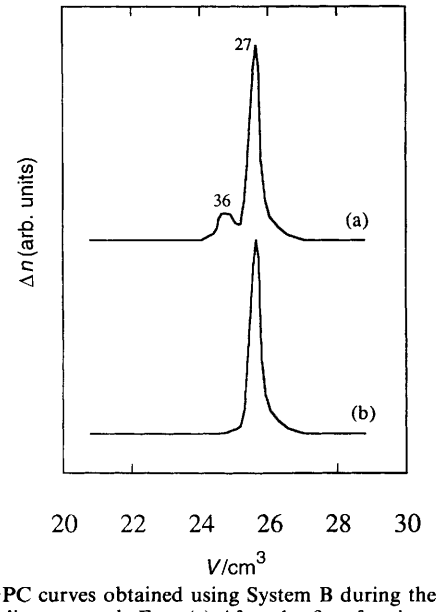

Fig. 3 GPC curves obtained using System B during the preparation of cyclic oligomer *cyclo*-E_{27}. (a) After the first fractionation by preparative GPC to obtain *cyclo*-E_{27}-1. (b) After a second fractionation by preparative GPC to obtain *cyclo*-E_{27}. The constituents of *cyclo*-E_{27}-1 are indicated in (a).

Accordingly *cyclo*-E_{27}-1 was re-fractionated by preparative GPC to obtain a fraction, denoted *cyclo*-E_{27}, the GPC curve of which is shown as curve (b) in Fig. 3.

2.5 α-Methyl, ω-methoxyheptacosa(oxyethylene) ($C_1E_{27}C_1$)

Methylation of E_{27} was by reaction with iodomethane under Williamson conditions as described previously.[32,33] Powdered KOH (0.62 g) was stirred with chlorobenzene (20 cm^3) and iodomethane (0.82 g, 5.8×10^{-3} mol) before addition (over 15 min) of a solution of E_{27} (0.50 g, 4.1×10^{-4} mol) in warm chlorobenzene (10 cm^3), followed by further stirring for 8 h at room temperature. After filtration, the solution was rotary evaporated to a small volume. Dichloromethane (30 cm^3) was added and the solution washed with distilled water (10×10 cm^3) to remove all residual iodide (tested by acidification and addition of $AgNO_3$). After concentration of the organic phase, the product was melt evaporated (24 h, 10^{-3} mm Hg). The IR spectrum showed no significant absorption at 3600–3200 cm^{-1}: quantitative assessment[31] indicated >99% conversion to dimethyl ether.

Preparative GPC was used to obtain a first fraction, denoted $C_1E_{27}C_1$-1. Analytical GPC using System B showed the presence of higher oligomers characterised as $C_1E_{36}C_1$ and $C_1E_{45}C_1$: see curve (a) in Fig. 4. Accordingly $C_1E_{27}C_1$-1 was re-fractionated by preparative GPC to obtain a fraction denoted $C_1E_{27}C_1$: see curve (b) in Fig. 4.

2.6 Sample purity by NMR

Samples dissolved in $CDCl_3$ were examined by ^{13}C NMR spectroscopy using a Bruker AC300E spectrometer operating at 75.5 MHz. Spectra of purified samples of *cyclo*-E_{27}, $C_1E_{27}C_1$ and purified precursor E_{27} are illustrated in Fig. 5. Assignments, taken from Heatley *et al.*,[34] are $\delta = 70.3$ (internal $-OCH_2CH_2O-$), $\delta = 72.0$ ($-OCH_2CH_2OCH_3$), $\delta = 58.8$ ($-OCH_2CH_2OCH_3$), $\delta = 72.5$ ($-CH_2CH_2OH$) and $\delta = 61.5$ ($-OCH_2CH_2OH$). In the case of *cyclo*-E_{27}, a single resonance at $\delta = 70.3$ confirmed the absence of end groups. The integrated resonances from end groups and chain groups obtained from the spectrum of $C_1E_{27}C_1$ were consistent with expectation. The characteristics of the four samples that were studied further are summarised in Table 1.

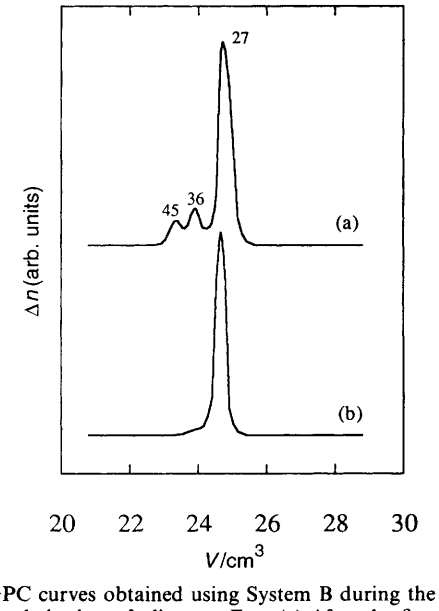

Fig. 4 GPC curves obtained using System B during the preparation of the dimethyl ether of oligomer E_{27}. (a) After the first purification by preparative GPC to obtain $C_1E_{27}C_1$-1. (b) After a second fractionation by preparative GPC to obtain $C_1E_{27}C_1$. The constituents of $C_1E_{27}C_1$-1 are indicated in (a).

Table 1 Molecular characteristics of the samples

sample	chain length (NMR)	purity (%)	impurities
cyclo-E_{27}	—	>99	—
$C_1E_{27}C_1$	$E_{26.9}$	>98	$C_1E_{36}C_1$
cyclo-E_{27}-1	—	*ca.* 90	*cyclo*-E_{36}
$C_1E_{27}C_1$-1	$E_{30.0}$	*ca.* 80	$C_1E_{36}C_1$, $C_1E_{45}C_1$

3. Experimental methods

3.1 Simultaneous WAXS/SAXS/DSC

Measurements were made on beamline 8.2 of the SRS at the CCLRC Daresbury Laboratory, Warrington, UK. Details of the storage ring, radiation (λ = 1.5 Å) and camera geometry and data collection electronics have been given elsewhere.[35] The camera was equipped with a multiwire quadrant detector (SAXS) located 3.5 m from the sample position and a curved knife-edge detector (WAXS) which covered 120° of meridional arc at a radius of 0.3 m. A vacuum chamber placed between the sample and detectors reduced air scattering and absorption. The scattering pattern from an oriented specimen of wet collagen (rat-tail tendon) was used to calibrate the SAXS detector, and high-density polyethylene, aluminium and an NBS silicon standard were used to calibrate the WAXS detector. The experimental data were corrected for background scattering (subtraction of the scattering from the camera, hot stage and an empty cell), sample thickness and transmission, and for any departure from positional linearity of the detectors.

The specimens for SAXS/WAXS were placed in a TA Instruments DSC pan containing a 0.75 mm brass spacer ring and fitted with windows (*ca.* 7 mm diameter) made from 25 μm thick mica. The loaded pans were placed in the cell of a Linkam DSC of single-pan design, which enabled samples to be melted and recrystallised *in situ*. More complete descriptions of this aspect of the apparatus can be found elsewhere.[36,37] In the present experiments, the samples taken from storage were cooled to 5 °C, melted by heating to 50–60 °C at either 5 or 10 K min^{-1}, and recrystallised by cooling at 5 or 10 K min^{-1} back to 5 °C. The beam-line data acquisition system had a time-frame generator programmed to collect the SAXS/WAXS data in 6 s frames separated by a wait-time of 10 μs.

Results were presented as intensity *vs.* scattering angle 2θ (WAXS, normalised to Cu-Kα radiation) or intensity *vs.* scattering vector $q = (4\pi/\lambda)\sin\theta$ (SAXS). Long spacings were calculated from the position (q^*) of the first-order maximum in the Lorentz-corrected intensity (Iq^2) *vs.* q (*i.e.* $d = 2\pi/q^*$) and checked against the positions of higher-order maxima.

The essentially one-dimensional geometry of the SAXS system made it ideal for samples which were isotropic with respect to X-ray scattering. This was readily achieved in previous experiments on polydisperse samples which crystallised in grains of small size relative to the sample.[23,24] However the present samples formed relatively large layer crystals which orientated with respect to the mica windows of the specimen pans. This meant that WAXS reflections could lie off the meridian and out of range of the knife-edge detector, making collection of a representative pattern impossible. Accordingly, the WAXS results were supplemented by use of a flat-plate camera (see Section 3.2). The simpler diffraction patterns from the long spacings were reasonably well sampled by the SAXS quadrant detector, although overall scattering intensities were found to vary between replicate experiments and on recrystallisation of a given sample.

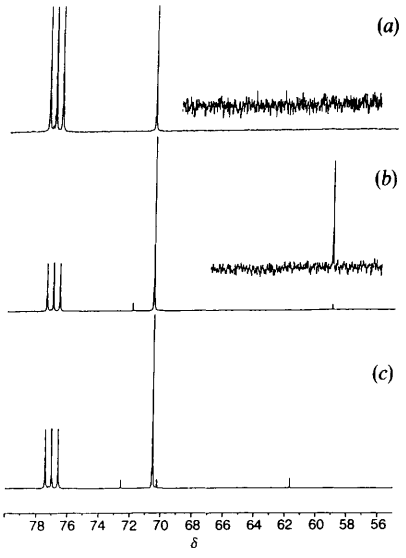

Fig. 5, ^{13}C NMR spectra of purified samples of (a) *cyclo*-E_{27}, (b) $C_1E_{27}C_1$ and (c) E_{27}. The triplet centred on δ 77 is from the solvent. The expansion of spectrum (a) shows no evidence of end groups, and that of spectrum (b) shows no evidence of hydroxy end groups.

3.2 WAXS (flat-plate camera)

X-ray diffraction patterns were recorded photographically (Kodak KP79846-B) by means of a flat-plate camera and nickel-filtered Cu-Kα radiation (λ = 1.54 Å) from a Philips PW1130/00 fine-focus tube operated at 40 kV and 20 mA. Dry samples were sealed into thin-walled capillaries (0.3 mm i.d.) and crystallised at room temperature. The sample-to-film distance was 6 cm, and the exposure time was 4 h. Calibration was with powdered NaCl.

3.3 Raman spectroscopy

Raman scattering at 90° to the incident beam was recorded by means of a Spex Ramalog spectrometer fitted with a 1403 double monochromator, and with a third (1442U) monochromator operated in scanning mode. The light source was a Coherent Innova 90 argon-ion laser operated at 514.5 nm and 400 mW. Typical operating conditions for the low-frequency range were bandwidth 1.5 cm^{-1}, scanning increment 0.05 cm^{-1}, integration time 4 s, and for the high-frequency range were bandwidth 2.5 cm^{-1}, scanning increment 1 cm^{-1}, integration time 3 s. The low-frequency scale was calibrated by reference to the 9.6 and 14.9 cm^{-1} bands in the low frequency spectrum of L-cystine. High frequency spectra were generally recorded for each sample before and after recording the low-frequency spectra, and so served to confirm the stability of the samples under the conditions of the experiments, as well as giving valuable structural information.

Samples were enclosed in capillary tubes, melted, and then cooled rapidly to room temperature to crystallise. Spectra were recorded with the samples at -10 ± 1 °C (achieved by means of a Harney–Miller cell, Spex Industries Inc.). The exact temperature of the Raman experiment was unimportant as the temperature derivative of frequency is known to be small for the LAM bands of low-molar-mass poly(oxyethylene)s.[18]

3.4 Differential scanning calorimetry

A Perkin-Elmer DSC-4 was used. Known weights (5–10 mg) of the samples, which had been stored either at room temperature or in a freezer at −10 °C, were sealed into aluminium pans. All samples were cooled to 0 °C in the calorimeter before heating at 5 K min^{-1} through the melting point to 70–80 °C. The sample was then cooled to a temperature well below the

melting point and, after a period for equilibration, the heating process was repeated. The experiment was repeated with other heating rates. Values of the enthalpy of fusion were obtained from peak areas, and apparent melting temperatures were obtained from the temperature at the maximum of the peak. The power and temperature scales of the calorimeter were calibrated against the enthalpies of fusion and melting temperatures of pure indium and of organic standards melting in the appropriate range.

4. Results and Discussion

Samples of *cyclo*-E_{27} and $C_1E_{27}C_1$ were thoroughly investigated by X-ray scattering, Raman spectroscopy and DSC. Corresponding measurements made on less pure samples (*cyclo*-E_{27}-1 and $C_1E_{27}C$-1) are described in Section 4.5.

4.1 WAXS

The WAXS patterns obtained for crystalline *cyclo*-E_{27} and $C_1E_{27}C_1$ at the CCLRC Daresbury Laboratory were similar to one another and to the pattern expected[27] for crystalline poly(oxyethylene), *i.e.* for oxyethylene chains packed as alternate right- and left-handed helices. WAXS from linear uniform oligo(oxyethylene)s has been described previously.[15,16] A WAXS pattern obtained for *cyclo*-E_{27} is shown in Fig. 6, where the major reflections at $\theta = 9.6$ and 11.7° are clearly seen. Within the error of determination all reflections detected could be indexed by the usual monoclinic sub-cell.[27] Similar patterns (not illustrated) were obtained with the flat-plat camera.

4.2 High-frequency Raman spectroscopy

High frequency spectra recorded for crystalline *cyclo*-E_{27} and $C_1E_{27}C_1$ are shown in Fig. 7. These spectra are similar to one another and to those published previously for poly(oxyethylene) and related oligomers.[38–40] Observation of the indicator bands at 281 (*cyclo*-E_{27}), 278 ($C_1E_{27}C_1$), 363, 392 and 1232 cm^{-1} provided evidence of the helical structure of the oligo(oxyethylene) chain in the crystalline cyclic and linear oligomers. The difference in frequency between 281 and 278 cm^{-1} was observed (within an uncertainty of 1 cm^{-1}) for all spectra recorded, and is consistent with different lengths of helical sequences in the two oligomers. A previous study[41] has shown that this vibration is associated with a transverse breathing mode of the uniform helix, and that its frequency should decrease with an increase in helix length. The observed frequencies show that crystalline *cyclo*-E_{27} contained shorter uniform helical sequences than crystalline $C_1E_{27}C_1$.

The spectrum of *cyclo*-E_{27} showed ill-defined weak bands on the lower-frequency side of 842 and 1063 cm^{-1} which are missing in the spectrum of $C_1E_{27}C_1$: see Fig. 7. These bands

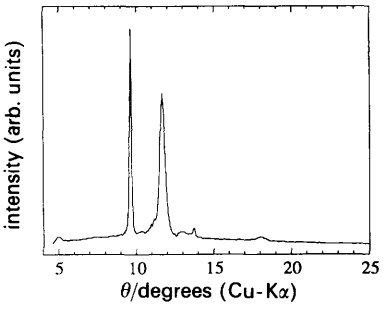

Fig. 6 WAXS pattern from crystalline *cyclo*-E_{27} ($T = 20$ °C). The intense reflection at Bragg angle $\theta = 9.66°$ [indexed (120)] and the composite reflection at $\theta = 11.66°$ [indexed (112) and (032) among others] are characteristic of crystalline poly(oxyethylene).[27]

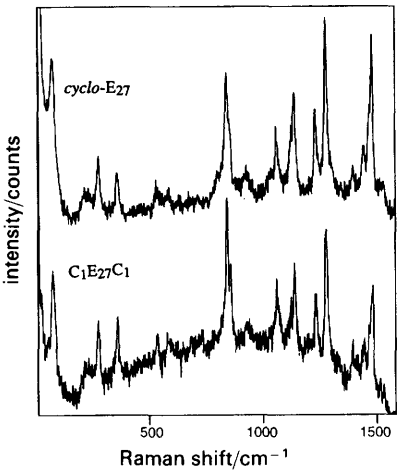

Fig. 7 High-frequency Raman spectra of crystalline oligomers *cyclo*-E_{27} and $C_1E_{27}C_1$ ($T = -10$ °C). For clarity of presentation the intensity scales of the two spectra are displaced relative to one another.

are ascribed to vibrations of parts of the chain which are not in uniform helical conformation, and are possibly associated with the chain folds of crystalline *cyclo*-E_{27}.

4.3 Small-angle X-ray scattering

SAXS patterns obtained for crystalline *cyclo*-E_{27} and $C_1E_{27}C_1$ at 20 °C are shown in Fig. 8. Two reflections are apparent in each pattern, the spacings of which are consistent with reflections from the long spacings of layer crystals. The derived long spacings (*d*, listed in Table 2) are 39 and 81 Å respectively. The estimated error is ± 2%. Calculated molecular lengths assuming a long spacing of 2.85 Å per E unit[42] are 78 Å (*cyclo*-E_{27}) and 80 Å ($C_1E_{27}C_1$), the difference being the two methyl groups of the latter oligomer. An interlayer gap of *ca.* 1 Å might be expected.[43] Accordingly, the calculated spacing for oligomer $C_1E_{27}C_1$ matches that observed. Similarly, the spacing of $d = 39$ Å obtained for *cyclo*-E_{27} is essentially that predicted for a helical oxyethylene chain of half the molecular length, consistent with the folded-chain conformation illustrated in Section 1.

4.4 Low-frequency Raman spectroscopy

Low-frequency Raman spectra of crystalline *cyclo*-E_{27} and $C_1E_{27}C_1$ are shown in Fig. 9. The broad peak at 80 cm^{-1} is characteristic of crystalline helical oligo(oxyethylene) chains.[17–19,44] The prominent peaks at low frequency are assigned to LAM-1, and their frequencies are so listed in

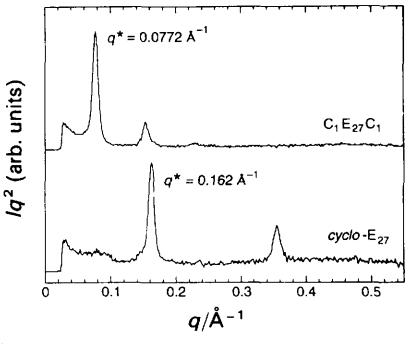

Fig. 8 SAXS patterns from crystalline oligomers *cyclo*-E_{27} and $C_1E_{27}C_1$ ($T = 20$ °C). The q values at the first-order reflections from the long spacings are marked. For clarity of presentation the Lorentz-corrected intensity scales of the two patterns are displaced relative to one another.

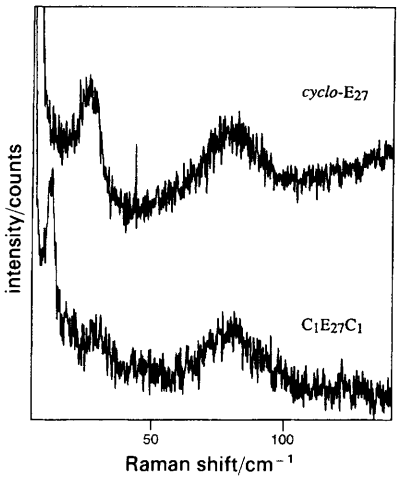

Fig. 9 Low-frequency Raman spectra (5–140 cm^{-1}) of crystalline *cyclo*-E_{27} and linear $C_1E_{27}C_1$ (as indicated). For clarity of presentation the intensity scales of the two spectra are displaced relative to one another.

Table 2. In Fig. 10, the LAM-1 frequencies found for the present samples and those reported[19] for other linear oligo(oxyethylene)s are plotted against reciprocal stem length in E units or equivalent (z), taking this to be the chain length of a linear oligomer and half the chain length of a cyclic oligomer: *i.e.* $z = n + 1$ for $C_1E_nC_1$ and $n/2$ for *cyclo*-E_n. Results[19] for oligomers $C_1E_9C_1$ and $C_1E_7C_1$ are not included in Fig. 10 since the layer spacing from SAXS and the LAM-1 from Raman spectroscopy are anomalous for these oligomers, consistent with helices tilted with respect to the end-group plane.

The good agreement between previous and present results seen in Fig. 10 confirms that the present linear oligomer ($C_1E_{27}C_1$) crystallised in a unfolded helical conformation, and the cyclic oligomer (*cyclo*-E_{27}) in a twice-folded helical conformation. In other words, the results from low-frequency Raman spectroscopy confirm the conclusion drawn from the SAXS patterns.

4.5 Effect of oligomeric impurities

The effect of oligomeric impurities on the SAXS and Raman results was of interest to us. Accordingly, additional measurements of long spacing and LAM-1 frequency were made for the less-pure samples *cyclo*-E_{27}-1 and $C_1E_{27}C_1$-1. These results are listed in Table 3, and can be compared with those obtained for the pure oligomers listed in Table 2. The LAM-1 frequency was little affected by the presence of a small fraction of other oligomers, presumably reflecting the fact that the position of the peak of the signal in the spectrum corresponded to the vibrational frequency of the major component. By contrast the long spacing from SAXS was sensitive to oligomeric impurities, as might be expected since the SAXS experiment yields a number average over the long spacings of the crystals in the sample.

Table 2 Results of SAXS, low-frequency Raman spectroscopy and DSC: purified oligomers[a]

sample	d/Å (SAXS)	ν_1/cm^{-1} (Raman)	T_m/°C (DSC)	$\Delta_{fus}H(T_m)$/J g^{-1} (DSC)
cyclo-E_{27}	39	26	41	131
$C_1E_{27}C_1$	81	12.1	42	182

[a] SAXS at 20 °C, Raman at −10 °C.

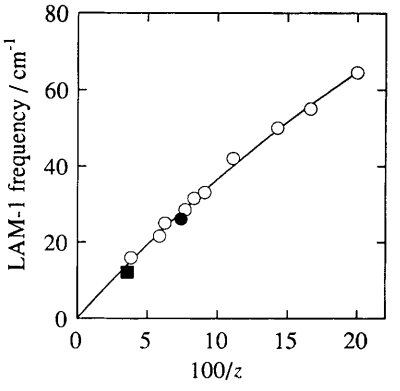

Fig. 10 LAM-1 frequencies *vs.* $1/z$ for cyclic and linear oligo(oxyethylene)s ($z = n + 1$ for linear oligomers $C_1E_nC_1$ and $n/2$ for *cyclo*-E_n). (○) $C_1E_nC_1$ from ref. 19; (■) $C_1E_{27}C_1$ and (●) *cyclo*-E_{27} from present work.

4.6 Thermal analysis by the temperature dependence of SAXS

4.6.1 Long spacing. In Fig. 11 the long spacings (d) for *cyclo*-E_{27} and $C_1E_{27}C_1$ are plotted against frame count (1 frame = 6 s) during the heating-cooling cycle 15 °C → 45 °C (hold for 1 min) → − 5 °C at a ramp rate of 5 K min^{-1}. As can be seen, for *cyclo*-E_{27} d was constant (39 ± 1 Å) for the heated crystalline oligomer to melting and returned to the same constant value upon recrystallisation. For $C_1E_{27}C_1$ d increased as temperature was increased above 30 °C (from 81 to 86 Å) and correspondingly decreased on cooling the recrystallised sample (from 90 to 84 Å). The variation of d found for the linear oligomer is attributed to end melting as the temperature approaches the melting point. This effect, suggested by Mandelkern and considered for *n*-alkanes by Flory and Vrij[45] was well illustrated in a study of the melting behaviour of $C_{44}H_{90}$ and $C_{94}H_{190}$ by Kim and Mandelkern,[46] which showed that end melting occurred for the longer oligomer but not for the shorter. In the present case, end melting could result in a proportion of the oligomer being transformed from the helical to the *trans*-planar conformation, with a corresponding small increase in long spacing.

Judged by the behaviour of d illustrated in Fig. 11, melting of the two oligomers occurred at a similar time in the heating cycle (frame 53–54) corresponding to $T_m \approx 42$ °C, while the crystallisation temperatures of the samples were some 10–13 K lower than their melting points, the linear oligomer having the smaller undercooling for crystallisation. Thermal lag was known to be small in the WAXS/SAXS/DSC experiments.[36,37]

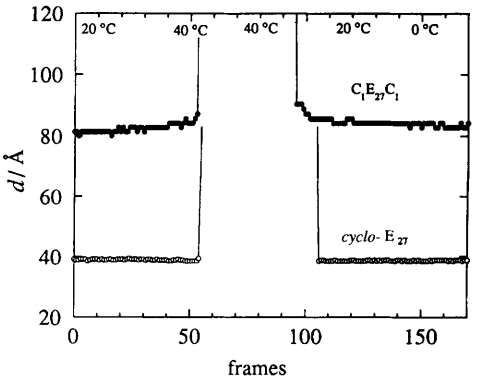

Fig. 11 SAXS from crystalline oligomers *cyclo*-E_{27} and $C_1E_{27}C_1$ (as indicated). The data are long spacing (d) *vs.* frame count (1 frame = 6 s, heating/cooling rate = 5 K min^{-1}). The temperature program was: heat from 15 to 45 °C (frames 0–60), maintain at 45 °C (frames 60–70), cool from 45 to − 5 °C (frames 70–170).

Table 3 Results of SAXS and low-frequency Raman spectroscopy impure oligomers[a]

sample	d/Å (SAXS)	ν_1/cm^{-1} (Raman)
cyclo-E_{27}-1	39	26
$C_1E_{27}C_1$-1	90	11.6

[a] SAXS at 20 °C, Raman at −10 °C.

4.6.2 Relative invariant. A SAXS invariant (Q', arbitrary units) was calculated throughout each heating/cooling experiment as the area under the Lorentz-corrected intensity *vs.* q curve between the first reliable data point, $q = 0.03$ Å^{-1}, and the limit of the SAXS experiments, $q \approx 0.50$ Å^{-1}. It has been shown[47] that the major contributions to the absolute invariant are well represented in Q'.

In Fig. 12, values of Q' obtained for *cyclo*-E_{27} and $C_1E_{27}C_1$ are plotted against frame count through the heating–cooling cycle. For a two-phase system the invariant can be discussed *via* the equation

$$Q = \phi_c(1 - \phi_c)\langle\Delta\eta^2\rangle \quad (1)$$

which is quadratic in the volume fraction of crystalline material (ϕ_c) and linear in the electron density difference term ($\langle\Delta\eta^2\rangle$) from which the SAXS pattern originates. For a completely crystallisable oligomer, eqn. (1) does not apply, and Q' reflects the electron density deficiency at the interlayer gap and has a linear temperature dependence. The straight lines drawn on Fig. 12 draw attention to those parts of the Q'–T curves which fulfil that condition. If the layers are incompletely crystalline, *i.e.* end melted, then the additional contribution resulting from the difference in electron density between the crystal stem and the liquid-crystal ends follows the form of eqn. (1) with ϕ_c progressively decreasing as temperature is increased.

The linear increase in Q' with T found on initially heating *cyclo*-E_{27} is consistent with high crystallinity ($\phi_c \approx 1$) and Q' varying linearly with temperature because of the difference in thermal expansion across the crystalline layer (helix) and the van der Waals gap. Melting started slowly at *ca.* 35 °C and finished abruptly at 42 °C (where $\phi_c = 0$). Crystallisation, started at *ca.* 30 °C, seen in Fig. 12 as a steep sigmoidal curve rising to a relatively high value consistent with initial formation on rapid cooling of a lamella crystal with disordered surface layers. The value of Q' characteristic of a well-ordered layer crystal (*e.g.* frame 0 in Fig. 12) was regained after *ca.* 30 min at low temperature.

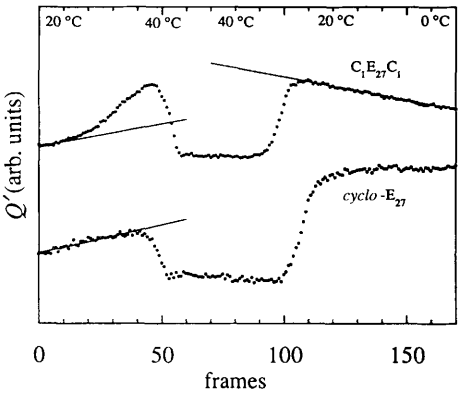

Fig. 12 SAXS from crystalline oligomers *cyclo*-E_{27} and $C_1E_{27}C_1$ (as indicated). Integrated intensity of scattering (Q') *vs.* frame count. 1 frame = 6 s, heating/cooling rate = 5 K min^{-1}. Temperature program: heat from 15 to 45 °C (frames 0–60), maintain at 45 °C (frames 60–70), cool from 45 to −5 °C (frames 70–170). The ordinate scales of the plots are arbitrarily scaled and are displaced relative to one another. See text for explanation of the straight lines drawn through the points.

As seen in Fig. 12, the Q'–T behaviour of $C_1E_{27}C_1$ differed significantly from that of *cyclo*-E_{27}. At the lowest temperatures the change in Q' was similar to that found for *cyclo*-E_{27}, and the layers can be characterised as completely crystalline. On heating above 25 °C the value of Q' increased sharply above that expected if $\phi_c \approx 1$, consistent with end melting, before falling away to $\phi_c = 0$ at the melting point (*ca.* 43 °C). The crystallisation curve was similar to that found for *cyclo*-E_{27}, but the process started earlier in the cooling cycle, and the linear fall in Q' with T below 25 °C indicated rapid formation of well-ordered crystals in the primary process.

4.7 Thermal analysis by DSC

DSC curves obtained for *cyclo*-E_{27} and $C_1E_{27}C_1$ at a heating rate of 5 K min^{-1} are shown in Fig. 13. Stored samples and those freshly crystallised gave similar results, as did experiments at different heating rates. In particular, a small peak at 30 °C in the DSC curve of the linear oligomer (*ca.* 4% of the total area) was not eradicated by slow heating. It is likely that the events observed in the melting of $C_1E_{27}C_1$ (*i.e.* the small melting peak in DSC and the variation of d and Q' in SAXS/DSC) have a common origin in the onset of end melting. The general features of the melting behaviour described in Section 4.6 are well reproduced by the onset and peak temperatures obtained by DSC. On cooling in the DSC at 5 K min^{-1} crystallisation of the two oligomers was detected at undercoolings of *ca.* 10–14 K, also in good agreement with the results from SAXS *vs.* T.

The width of the melting peaks in DSC (see Fig. 13) resulted in large part from thermal lag. This was verified by plotting the width at half height ($\Delta T_{1/2}$) against the square root of the heating rate[48] and extrapolating to zero heating rate: see, for example, Fig. 14(a). Within an uncertainty of ±0.3 K, the data extrapolate to 0 K, as indicated by the line drawn through the origin. This result confirms the high purity of the sample. In a similar way, values of T_m were corrected for thermal lag by plotting temperature at the peak of the endotherm against the square root of the heating rate and extrapolating to zero heating rate: see, for example, Fig. 14(b).

Values of T_m (extrapolated as described above) and of $\Delta_{fus}H$ (averaged over several determinations, and including the minor peak for sample $C_1E_{27}C_1$) are listed in Table 4.

4.8 Thermodynamics of formation of end and fold planes

In considering values of $\Delta_{fus}H$ it is important to allow for the difference in specific heat capacity between crystal and melt,

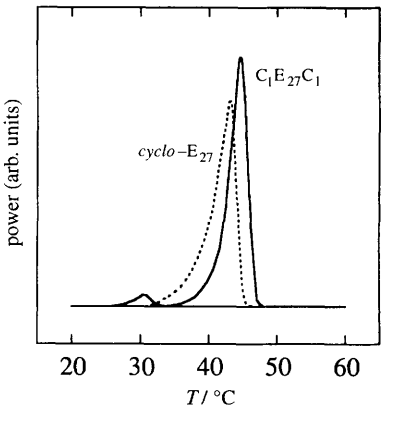

Fig. 13 DSC curves for oligomers *cyclo*-E_{27} and $C_1E_{27}C_1$ (as indicated)

Table 4 Enthalpies of fusion of linear oligo(oxyethylene)s

oligomer	T_m/°C	$\Delta_{fus}H(T_m)$/J g^{-1}	$\Delta_{fus}H$(40 °C)/J g^{-1}	ref.
$C_1E_8C_1$	3	151	171	53
$C_1E_9C_1$	16	168	180	50
$C_1E_{15}C_1$	29	172, 175	177, 180	51, 53
$C_1E_{17}C_1$	28	172	178	52
$C_1E_{18}C_1$	32	187	191	52
$C_1E_{25}C_1$	43	183, 188	182, 187	53
$C_1E_{27}C_1$	42	182	181	this work
$C_1E_{45}C_1$	51	185	179	20

ΔC_p. As reported previously,[49] values of ΔC_p for uniform oligo(oxyethylene) dimethyl ethers measured at a given temperature are essentially independent of chain length, and are well represented by

$$\Delta C_p = 0.650 - 5.06 \times 10^{-3}T \quad (2)$$

where ΔC_p is in J K^{-1} g^{-1} and T is in °C. Consequently, the specific enthalpy of fusion of a given oligomer at a given temperature (T) is given by

$$\Delta_{fus}H(T) = \Delta_{fus}H(T_m) + 0.650(T_m - T) - 2.53 \times 10^{-3}(T_m^2 - T^2) \quad (3)$$

where $\Delta_{fus}H(T_m)$ is the measured specific enthalpy of fusion. Values of $\Delta_{fus}H(T_m)$ reported here and elsewhere[20,50–53] for several uniform linear oligo(oxyethylene) dimethyl ethers are listed in Table 4, together with the values corrected to 40 °C. A standard temperature of 40 °C was chosen since this was the approximate melting temperature of *cyclo*-E_{27}, and was also well within the range of the melting points of all the oligomers under consideration (see Table 4). This procedure minimised the possibility of serious error in making the corrections.

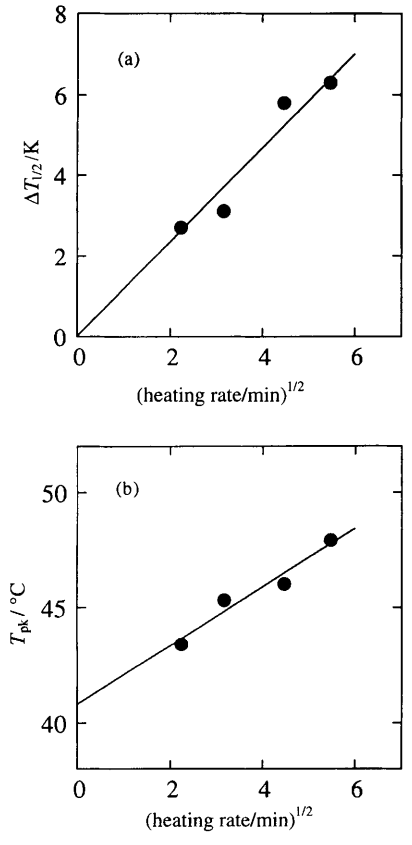

Fig. 14 DSC of oligomer *cyclo*-E_{27}. (a) Width of DSC peak at half height *vs.* square root of heating rate. (b) Temperature at the peak *vs.* square root of heating rate.

Values of $\Delta_{fus}H$(40 °C) from Table 4 and a similarly-corrected value for *cyclo*-E_{27} were multiplied by the molar mass of an E unit (44 g mol^{-1}) and plotted against the reciprocal stem length in E units ($1/z$): see Fig. 15. It was assumed that ΔC_p for the cyclic oligomer was equal to that found for the linear oligomers. Stem length z is defined in Section 4.4.

For layer crystals the enthalpy of fusion per chain unit should conform to the equation

$$\Delta_{fus}H = \Delta_{fus}H^0 - (2\eta_e/z) \quad (4)$$

where $\Delta_{fus}H^0$ is the thermodynamic enthalpy of fusion in J (mol of chain units)$^{-1}$, η_e is the enthalpy of formation of the chain end or fold plane from perfect crystal, measured in J (mol of crystal stems)$^{-1}$. The least-squares straight line through the points for the linear oligomers is shown in Fig. 15. In constructing this line the data points for $C_1E_{45}C_1$ and $C_1E_9C_1$ were omitted. The former is known to be end melted well below its crystal melting temperature,[53] and the latter to crystallise with helices tilted with respect to the end-group plane (see Section 4.4). The intercept of the line gives $\Delta_{fus}H^0$(40 °C) = 8.4 ± 0.2 kJ mol^{-1}, which corresponds to 191 ± 5 J g^{-1} at 40 °C or, *via* eqn (3), to 208 ± 5 J g^{-1} at 70 °C. The slope of the line gives η_e = 3.9 ± 1.6 kJ mol^{-1}. A positive value of η_e correctly accords with a low intermolecular energy in the end plane compared with the bulk of the crystal.

The obtained value of $\Delta_{fus}H^0$ = 208 ± 5 J g^{-1} at 70 °C is in good agreement with a previous determination of 209 J g^{-1} by a diluent method applied to high molar mass poly(oxyethylene) in a manner which avoided use of polymer solution theory, *i.e.* by determining solute activity from solvent activity *via* the Gibbs-Duhem relationship.[54] Others have used polydisperse samples and DSC to determine $\Delta_{fus}H^0$(70 °C), which method introduces additional uncertainty but nevertheless yields comparable values: *e.g.* 197 J g^{-1} by Buckley and Kovacs,[55] 218 J g^{-1} by Romankevich and Frenkel.[56]

The point of interest here is the large difference in the enthalpies of fusion obtained for *cyclo*-E_{27} and a linear oligo(oxyethylene) of equivalent stem length. To illustrate this difference the data point obtained for *cyclo*-E_{27} is shown in Fig. 15. Given the stem length involved, the reduction in $\Delta_{fus}H$ compared with $\Delta_{fus}H^0$ leads to $\eta_e \approx 18$ kJ mol^{-1}, implying (since each fold involves two crystal stems) an enthalpy of formation of a fold from perfect crystal of *ca.* 36 kJ (mol of folds)$^{-1}$ at 40 °C. The uncertainty in these values is estimated to be ±20%. These results are discussed further below.

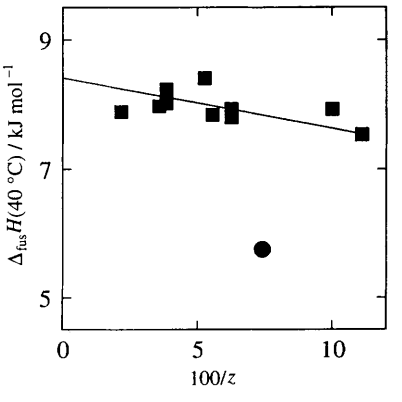

Fig. 15 $\Delta_{fus}H$ corrected to 40 °C *vs.* $1/z$ for (■) linear oligomers $C_1E_nC_1$ and (●) *cyclo*-E_{27} ($z = n + 1$ for linear oligomers $C_1E_nC_1$ and $n/2$ for *cyclo*-E_n). The points for $C_1E_{45}C_1$ and $C_1E_9C_1$ were ignored in deriving the least-squares straight line through the points for the linear oligomers (see text).

Analysis of the melting temperatures is more complicated. For the linear oligomers we assume end pairing, in the sense described by Flory and Vrij,[45] and write (in a form used previously[57] but with present notation)

$$T_m = \frac{T_m^0[1 - (2\gamma_e/\Delta_{fus}H^0 z)]}{1 - [RT_m^0 \ln(1/z)/\Delta_{fus}H^0 z]} \quad (5)$$

where T_m^0 is the thermodynamic melting temperature, $\Delta_{fus}H^0$ is the thermodynamic enthalpy of fusion, and γ_e is the Gibbs energy of formation of the chain end or fold planes of the layer crystal from perfect (bulk) crystal, measured in J (mol of crystal stems)$^{-1}$. The denominator in the RHS of eqn. (5) modifies the term often used in polymer physics to account for the effect of layer thickness on melting temperature in the absence of end pairing. Rearrangement of eqn. (5) gives a more convenient form

$$\frac{\Delta_{fus}H^0(T_m - T_m^0)}{T_m^0} - \frac{RT_m \ln(1/z)}{z} = -\frac{2\gamma_e}{z} \quad (6)$$

Substituting

$$\gamma_e = \eta_e - T_m\sigma_e \quad (7)$$

where σ_e is the molar entropy of formation of the chain end or fold planes of the layer crystal from perfect crystal, and rearranging gives

$$\frac{1}{T_m}\left[\frac{\Delta_{fus}H^0(T_m - T_m^0)}{T_m^0} - \frac{RT_m \ln(1/z)}{z} + \frac{2\eta_e}{z}\right] = \frac{2\sigma_e}{z} \quad (8)$$

which suggests a plot of the LHS against $1/z$ to obtain a value for σ_e: see Fig. 16. To do this the thermodynamic enthalpy of fusion was assumed to be correctly given by[49]

$$\Delta_{fus}H^0/\text{J g}^{-1} = 175 + 0.650T - 0.00253T^2 \quad (T \text{ in } ^\circ\text{C}) \quad (9)$$

(which is consistent with Fig. 14), and that the thermodynamic melting temperature is $T_m^0 = 70\,^\circ$C. The literature[55,56,58–60] gives values of T_m^0 in the range 69–78 °C, with a value towards the low end of that range being favoured.[61] The slope of the line drawn through the points for the linear oligomers in Fig. 16 (ignoring the points for oligomers $C_1E_{45}C_1$ and $C_1E_9C_1$, as discussed above) leads to a small negative value of $\sigma_e \approx -2.7$ J K^{-1} mol^{-1}.

In the analysis above, it was assumed that an E unit (or its equivalent) was equivalent to a segment as defined by Flory and Vrij.[45] If this is not the case, and if there are x segments in a chain of z units, then the probability that a segment chosen at random is an end segment is decreased by a factor z/x and, as a consequence, a term $R \ln(x/z)$ must be added to generate a true value of σ_e. If a chain atom represents a segment, then there are three chain atoms per unit in the present case, and the term to be added to σ_e is

$$R \ln(3) \approx 9 \text{ J K}^{-1} \text{ mol}^{-1} \quad (10)$$

sufficient to explain the negative value and to generate a small positive value of $\sigma_e \approx 6$ J K^{-1} mol^{-1}. This value is similar to that obtained by Flory and Vrij[45] in their analysis of the melting temperatures of the *n*-alkanes with z put equal to the number of chain atoms, *i.e.* $\sigma_e \approx +10$ J K^{-1} mol^{-1}.

Considering the melting of the cyclic oligomer, end pairing is not involved. In eqn. (5) the denominator was introduced to allow for end pairing arising from the need to choose one unit from z to place at the layer end plane.[45] If all units are available, then this term is unity and eqn. (8) reduces to

$$\frac{1}{T_m}\left[\frac{\Delta_{fus}H^0(T_m - T_m^0)}{T_m^0} + \frac{2\eta_e}{z}\right] = \frac{2\sigma_e}{z} \quad (11)$$

Solving eqn. (11) gives $\sigma_e \approx 39$ J K^{-1} mol^{-1}. To illustrate the difference between the cyclic and linear oligomers the data point obtained for *cyclo*-E_{27} is shown in Fig. 16. Taking eqn. (10) into account, the value of σ_e should be adjusted upwards to $\sigma_e \approx 48$ J K^{-1} mol^{-1}. Considering that there are two crystal stems per fold, the entropy increase on formation of chain folds from perfect crystal is $\sigma_e \approx 96$ J K^{-1} mol^{-1}. A realistic estimate of the uncertainty in σ_e is ±20%.

The results for the linear and cyclic oligomers show that the enthalpy and entropy increases associated with formation of chain folds from perfect crystal are very much larger than those associated with the formation of chain ends from perfect crystal. In Table 5 these quantities are compared with the thermodynamic enthalpy and entropy of fusion of poly(oxyethylene) per mole of E units. In these terms, it is seen that the formation of one chain fold is equivalent to the fusion of three or four crystalline E units, while the formation of two chain ends is equivalent to the fusion of one chain unit or less. This comparison should not be taken to mean that the folds in the cyclic oligomers are non-crystalline. The evidence from the temperature dependence of SAXS (presented in Section 4.6) shows that the layers are completely crystalline, *i.e.* that the folds have a fixed conformation.

It is likely that the chain folds in large crystalline *cyclo*-oligo(oxyethylene)s differ from those in large crystalline *cyclo*-alkanes, in which compact folds contain just four chain atoms.[4] A possible fold conformation for adjacent re-entry of an oxyethylene chain has been published previously.[62]. This involved three E units in a conformation of minimum energy, for which an intrachain fold energy of *ca.* 13 kJ mol^{-1} was calculated. No estimate was made of the decrease in interchain cohesive energy, but a significant contribution to the overall fold energy must be expected from that source. In this respect, it must be borne in mind that the oligo(oxyethylene) crystal structure is relatively complex and involves interpenetrating alternate right- and left-handed helices.

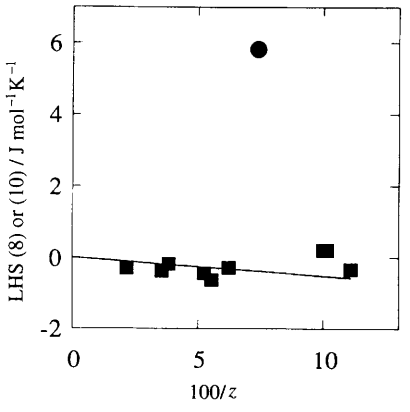

Fig. 16 Flory–Vrij plot [see eqn. (8)] for (■) linear oligomers $C_1E_nC_1$ and (●) *cyclo*-E_{27}. $z = n + 1$ for linear oligomers $C_1E_nC_1$ and $n/2$ for *cyclo*-E_n. The points for $C_1E_{45}C_1$ and $C_1E_9C_1$ were ignored in deriving the least-squares straight line through the points for the linear oligomers (see text).

Table 5 Thermodynamic quantities ($T = 40\,^\circ$C) for fusion of poly(oxyethylene) and for formation of chain ends (linear oligomers) and chain folds (cyclic oligomers) from perfect crystal

process	enthalpy increase/ kJ mol^{-1}	entropy increase/ J K^{-1} mol^{-1}
fusion (1 mol of E units)	8	27
chain ends (2 mol of ends)	8	12[a]
chain folds (1 mol of folds)	36	96[a]

[a] Assuming one segment = one chain atom: see text.

4.9 Comparison with results for other large crown ethers

Melting points have been reported for *cyclo*-E_{20} (60-crown-20), *i.e.* 46–50.5 °C by Chênevert and D'Astous,[6] and 57–58 °C by Gibson *et al.*[8] These temperatures are higher than $T_m \approx 41$ °C found in this work for *cyclo*-E_{27} (81-crown-27), but similar to those obtained for low-molar-mass cyclic poly(oxyethylene)s of number-average molar mass 1500–3000 g mol^{-1}, *i.e.* number-average *cyclo*-E_{34} to *cyclo*-E_{68}. It is noted that the samples prepared in other laboratories were not subject to the same rigorous purification and characterisation (particularly GPC, SAXS and Raman spectroscopy) procedures as was the present sample. The earlier preparations may have contained a significant proportion of higher oligomers.

Prof. H. W. Gibson kindly supplied the sample of *cyclo*-E_{10}. Mr. K. Nixon and Mr. P. Kobryn helped with the experimental work. The Engineering and Physical Research Council provided beamtime at CCLRC, where Dr. B. U. Komanschek helped with the WAXS/SAXS/DSC experiments. EPSRC, the British Council, the Japanese Ministry of Education, Science and Culture, and ICI Paints Plc provided financial assistance.

Note added in proof. Jointly with Prof. Gibson, we have now shown by both GPC and HPLC that the larger crown ethers prepared in Blacksburg were indeed mixtures including very large rings and catenanes.

References

1 M. Rothe and I. Rothe in *Polymer Handbook*, eds. J. Brandrup and I. H. Immergut, John Wiley, New York, 3rd edn., 1989, Section IV, p. 1.
2 K.-S. Lee and G. Wegner, *Makromol. Chem., Rapid Commun.*, 1985, **6**, 203.
3 K.-S. Lee, G. Wegner and S. L. Hsu, *Polymer*, 1987, **28**, 889.
4 G. Leiser, K.-S. Lee and G. Wegner, *Colloid Polym. Sci.*, 1988, **266**, 419.
5 W. Heitz, H. Höcker, W. Kern and H. Ullner, *Makromol. Chem.*, 1971, **150**, 73.
6 R. Chenevert and L. D'Astous, *J. Heterocyclic Chem.*, 1986, **23**, 1785.
7 C. A. Vitali and B. Masci, *Tetrahedron*, 1989, **45**, 2201.
8 H. W. Gibson, M. C. Behda, P. Engen, Y. X. Shen, J. Sze, H. Zhang, M. D. Gibson, Y. Delaviz, S. H. Lee, S. Liu, L. Wang, D. Nagvekar, J. Rancourt and L. T. Taylor, *J. Org. Chem.*, 1994, **59**, 2186.
9 B. Bömer, W. Heitz and W. Kern, *J. Chromatogr.*, 1970, **53**, 51.
10 A. Marshall, R. H. Mobbs and C. Booth, *Eur. Polym. J.*, 1980, **16**, 881.
11 H. H. Teo, R. H. Mobbs and C. Booth, *Eur. Polym. J.*, 1982, **18**, 541.
12 S. G. Yeates, H. H. Teo, R. H. Mobbs and C. Booth, *Makromol. Chem.*, 1984, **185**, 1559.
13 S. Kinugasa, H. Hayashi and S. Hattori, *Polym. J.*, 1990, **22**, 1059.
14 S. Kinugasa, A. Takatsu, H. Nakanishi, H. Nakahara and S. Hattori, *Macromolecules*, 1992, **25**, 4848.
15 A. Marshall, R. C. Domszy, H. H. Teo, R. H. Mobbs and C. Booth, *Eur. Polym. J.*, 1981, **17**, 885.
16 H. H. Teo, A. Marshall and C. Booth, *Makromol. Chem.*, 1982, **183**, 2265.
17 K. Viras, H. H. Teo, A. Marshall, R. C. Domszy, T. A. King and C. Booth, *J. Polym. Sci., Polym. Phys. Ed.*, 1983, **21**, 919.
18 K. Viras, T. A. King and C. Booth, *J. Polym. Sci., Polym. Phys. Ed.*, 1985, **23**, 471.
19 C. Campbell, K. Viras and C. Booth, *J. Polym. Sci., Polym. Phys. Ed.*, 1991, **29**, 1613.
20 S. G. Yeates and C. Booth, *Makromol. Chem.*, 1985, **186**, 2663.
21 G. Ungar, J. Stejny, A. Keller, I. Bidd and M. C. Whiting, *Science*, 1985, **229**, 386.
22 K. Viras, Z.-G. Yan, C. Price, C. Booth and A. J. Ryan, *Macromolecules*, 1995, **28**, 104.
23 G.-E. Yu, T. Sun, Z.-G. Yan, J. Cooke, K. Viras, A. J. Ryan and C. Booth, *Polymer*, in press.
24 T. Sun, G.-E. Yu, C. Price and C. Booth, J. Cooke and A. J. Ryan, *Polym. Commun.*, 1995, **36**, 3775.
25 Y.-Z. Yan, Z. Yang, C. Price and C. Booth, *Makromol. Chem., Rapid Commun.*, 1993, **14**, 725.
26 G.-E. Yu, P. Sinnathamby, C. Price and C. Booth, *Chem. Commun.*, 1996, 31.
27 Y. Takahashi and H. Tadokoro, *Makromolecules*, 1973, **6**, 881.
28 J. R. Craven, R. H. Mobbs, C. Booth, E. J. Goodwin and D. Jackson, *Makromol. Chem.*, 1989, **190**, 1207.
29 R. J. De Vos and E. Goethals, *Makromol. Chem., Rapid Commun.*, 1985, **6**, 53.
30 M. Ouchi, Y. Inoue, Y. Liu, S. Nagamune, S. Nakamura, K. Wada and T. Hakushi, *Bull. Chem. Soc. Jpn.*, 1990, **63**, 1260.
31 P. V. Wright and M. S. Beevers, in *Cyclic Polymers*, ed. J. A. Semlyen, Elsevier, London, 1986, ch. 3.
32 D. R. Cooper and C. Booth, *Polymer*, 1977, **18**, 164.
33 D. R. Cooper, Y.-K. Leung, F. Heatley and C. Booth, *Polymer*, 1978, **19**, 309.
34 F. Heatley, Y.-Z. Luo, J.-F. Ding, R. H. Mobbs and C. Booth, *Macromolecules*, 1988, **21**, 2713.
35 W. Bras, G. E. Derbyshire, A. J. Ryan, G. R. Mant, A. Felton, R. A. Lewis, C. J. Hall and G. N. Greaves, *Nucl. Instrum. Methods Phys. Res. Sect. A*, 1993, **326**, 587.
36 A. J. Ryan, *J. Therm. Anal.*, 1993, **40**, 887.
37 W. Bras, G. E. Derbyshire, S. Clarke, A. Devine, B. U. Komanschek, J. Cooke and A. J. Ryan, *J. Appl. Crystallogr.*, 1995, **28**, 26.
38 J. Maxfield and I. W. Shepherd, *Polymer*, 1975, **16**, 505.
39 H. Matsuura and K. Fukuhara, *J. Mol. Struct.*, 1985, **126**, 251.
40 H. Matsuura and K. Fukuhara, *J. Phys. Chem.*, 1987, **91**, 6139.
41 H. Matsuura and T. Miyazawa, *Bull. Chem. Soc. Jpn.*, 1969, **42**, 372.
42 J. R. Craven, H. Zhang and C. Booth, *J. Chem. Soc., Faraday Trans*, 1991, **87**, 1183.
43 T. G. E. Swales, H. H. Teo, R. C. Domszy, K. Viras, T. A. King and C. Booth, *J. Polym. Sci., Polym. Phys. Ed.*, 1983, **21**, 1501.
44 J. F. Rabolt, K. W. Johnson and R. N. Zitter, *J. Chem. Phys.*, 1974, **61**, 504.
45 P. J. Flory and A. Vrij, *J. Chem. Phys.*, 1963, **85**, 3548.
46 L. Mandelkern in *Comprehensive Polymer Science*, eds. C. Booth and C. Price, Pergamon, Oxford, 1989, vol. 2, ch. 11.
47 A. J. Ryan, W. Bras, G. R. Mant and G. E. Derbyshire, *Polymer*, 1994, **35**, 4537.
48 M. J. O'Neill, *Anal. Chem.*, 1964, **36**, 1238.
49 C. Campbell, K. Viras, M. J. Richardson, A. J. Masters and C. Booth, *Makromol. Chem.*, 1993, **194**, 799.
50 R. C. Domszy and C. Booth, *Makromol. Chem.*, 1982, **183**, 1051.
51 H. H. Teo, T. G. E. Swales, R. C. Domszy, F. Heatley and C. Booth, *Makromol. Chem.*, 1983, **184**, 861.
52 Z. Yang, PhD Thesis, University of Manchester, 1996.
53 M. J. Richardson, personal communication.
54 C. Booth, C. J. Devoy and G. Gee, *Polymer*, 1971, **12**, 327; C. J. Devoy, PhD Thesis, University of Manchester, 1966.
55 C. P. Buckley and A. J. Kovacs, *Prog. Colloid Polym. Sci.*, 1975, **58**, 44.
56 O. V. Romankevich and S. Ya. Frenkel, *Vysokomol. Soedin. Ser. A.*, 1980, **22**, 2416; *Polym. Sci. USSR*, 1980, **22**, 2647.
57 P. C. Ashman and C. Booth, *Polymer*, 1972, **13**, 459.
58 D. R. Beech and C. Booth, *J. Polym. Sci., Part B*, 1970, **8**, 731.
59 A. M. Affifi-Effat and J. N. Hay, *J. Chem. Soc., Faraday Trans. 2*, 1972, **68**, 656.
60 A. M. Rijke and S. McCoy, *J. Polym. Sci., Part A-2*, 1972, **10**, 1845.
61 C. Booth, in *Encyclopedia of Advanced Materials*, ed. D. Bloor, Pergamon, Oxford, 1994, p. 1815.
62 P. C. Ashman, C. Booth, D. R. Cooper and C. Price, *Polymer*, 1975, **16**, 897.

Paper 6/01637E; *Received 7th March*, 1996